clouds and from S. G. Warren *et al.* [*Technical Report DOE/ER 0406, NCAR/TN-17+SRT* (NCAR, Boulder, CO, December 1988] for low and cumulonimbus clouds. All clouds were assumed to be black. Cloud-base altitudes for low and cumulonimbus clouds were taken from Warren *et al.*'s atlas. We use ERBE outgoing LW radiation data as a constraint for adjusting the high cloud-top altitudes. We adjusted the ISCCP cloud-top altitudes for cirrus clouds until the computed TOA outgoing long-wave radiation for cloudy skies agreed with ERBE values within a few watts per square meter. This procedure amounted to increasing cirrus altitudes by about 4 km. The cloud thickness was assumed to be 1.5 km, except for cumulonimbus, where the cloud top was taken at 16-km altitude.

20. In this method, the computed values for $C_l(S)$ and $C_l(TOA)$ were used to estimate the ratio f_l, where $f_l = C_l(S)/C_l(TOA)$. The mean value of f_l for the WP region is about 0.3. The ratio increases from about 0.1 to 0.2 for cirrus clouds to about 0.9 for low clouds, yielding a mean value of 0.3. From ERBE data, the 5-year mean LW cloud forcing for the WP at TOA is 62 W m^{-2}. We estimated the 5-year annual mean $C_l(S)$ by letting $C_l(S) = f_l \times C_l(TOA) = 0.3 \times 62 \approx 19$ W m^{-2}.
21. TOGA-COARE cruise data were taken by an upward-looking calibrated pyrometer onboard the R/V *Vickers* from 2 February to 28 February 1994 in the WP at 156°E and the equator. The data and the techniques are as described [L. Schanz, thesis, Universität Hamburg, Germany (1994)].
22. G. S. Young, D. V. Ledvina, C. W. Fairall, *J. Geophys. Res.* **97**, 9595 (1992).
23. S. K. Esbensen and Y. Kushnir, *Technical Report 29* (Climate Research Institute, Oregon State University, Corvallis, 1981).
24. G. J. Zhang and M. J. McPhaden, *J. Climate*, in press.
25. The hourly data used for this comparison were collected from buoys located at 156°E and the equator; 156°E and 2°S; and 165°E and the equator. The time period covered by the hourly data is approximately from September 1992 to March 1993, including the TOGA-COARE period. The hourly fluxes were obtained by direct application of the bulk aerodynamic formulas to the hourly data. We obtained the fluxes from the daily averaged data by first averaging the hourly data to produce daily data and then applying the bulk aerodynamic formulas to the daily averaged data.
26. J. M. Oberhuber, *Technical Report 15* (Max-Planck-Institute for Meteorology, Hamburg, FRG, 1988).
27. R. T. Gosnell, C. W. Fairall, P. T. Webster, *Eos* **74: 43**, 125 (fall meeting suppl. 1993).
28. C. Gordon, *Philos. Trans. R. Soc. London Ser. A* **329**, 207 (1989).
29. P. R. Gent, *J. Geophys. Res.* **96**, 3323 (1991).
30. The spatial and temporal sampling errors should be within a few watts per square meter because of the massive amount of data values (at least 300,000 values) that had gone into the average. However, there may be potential errors, as large as 5 to 10 W m^{-2}, because of the algorithms used to convert satellite radiances to fluxes (J. A. Coakley, personal communication).
31. The model results shown in Fig. 3 use two independent radiation models. (i) DISORT is a comprehensive and computationally accurate multiple scattering code for the solar spectrum. This model is described in K. Stamnes *et al.*, *J. Atmos. Sci.* **38**, 387 (1988). (ii) Li *et al.* results shown in Fig. 3 use the model and algorithms described in Li *et al.* (*12*).
32. W. J. Wiscombe, R. M. Welch, W. D. Hall, *J. Atmos. Sci.* **41**, 1336 (1984); W. J. Wiscombe, *ibid.* **43**, 401 (1986). These papers suggest that the presence of large drops (radius > 100 μm) can enhance atmospheric absorption significantly. A thorough discussion of the controversies surrounding the so-called anomalous cloud absorption can be found in G. L. Stephens and S.-C. Tsay [*Q. J. R. Meteorol. Soc.* **116**, 671 (1990)].
33. J. T. Kiehl, *Phys. Today* **47**, 36 (November 1994).

24 August 1994; accepted 14 November 1994

Clustering and Periodic Recurrence of Microearthquakes on the San Andreas Fault at Parkfield, California

R. M. Nadeau, W. Foxall, T. V. McEvilly

The San Andreas fault at Parkfield, California, apparently late in an interval between repeating magnitude 6 earthquakes, is yielding to tectonic loading partly by seismic slip concentrated in a relatively sparse distribution of small clusters (<20-meter radius) of microearthquakes. Within these clusters, which account for 63% of the earthquakes in a 1987–92 study interval, virtually identical small earthquakes occurred with a regularity that can be described by the statistical model used previously in forecasting large characteristic earthquakes. Sympathetic occurrence of microearthquakes in nearby clusters was observed within a range of about 200 meters at communication speeds of 10 to 100 centimeters per second. The rate of earthquake occurrence, particularly at depth, increased significantly during the study period, but the fraction of earthquakes that were cluster members decreased.

Conceptual methods for earthquake forecasting and hazard mitigation depend critically on the process of fault slip being time-varying in a predictable manner, and evidence for such behavior has been elusive (*1*). In this report we describe patterns of microseismicity that show clustering in space, periodic recurrence, and systematic changes with time on the Parkfield stretch of the San Andreas fault, and we discuss possible mechanisms for this behavior.

Since 1987, seismicity near Parkfield, California, has been monitored with a network of sensitive seismographs installed in boreholes. This stretch of the San Andreas fault has experienced magnitude (M) 6 earthquakes on average every 22 years, on the basis of the record from 1857 to 1966 (*2*). Hypocenter locations for the last three events in the sequence define a common nucleation zone on the fault to within a few kilometers. A diverse earthquake prediction experiment is underway at Parkfield to establish a baseline of parameters that may reveal anomalous behavior before the next M 6 event (*3*).

Approximately 3000 earthquakes were recorded and located from January 1987 to June 1994 on the central 25-km-long section of the fault zone being studied. A three-dimensional model for *P* and *S* wave velocities for this segment has been developed from the microearthquake data (*4*). The small earthquakes are concentrated along a slipping fault zone that is characterized by locally depressed seismic wave velocities, particularly the shear-wave velocity (V_s), and by a region of elevated V_p/V_s near the presumed nucleation volume of the repeating M 6 earthquakes (V_p, *P* wave velocity).

Earth Sciences Division, Lawrence Berkeley Laboratory, and Seismographic Station, University of California, Berkeley, CA 94720, USA.

More than half of the earthquakes can be grouped spatially into small clusters within which events exhibit highly similar recorded waveforms, in many cases over the full 100-Hz bandwidth of the data (Fig. 1) (*5*). The generation of near-identical waveforms at wavelengths as short as 50 m suggests that the sources of seismic wave radiation for these clustered events are essentially repeating ruptures on a common slip surface. We are dealing mainly with small earthquakes in the magnitude range 0 to 1 on fault surfaces with dimensions of a few meters (*6*). The largest events studied have conventionally estimated source dimensions of a few tens of meters, although it is possible that the source dimension has been overestimated because of attenuation effects (*7*). Within the individual clusters, where relative location resolution is a few meters, we can study fault zone dynamics at a scale approaching that of large laboratory experiments.

To analyze the clustering phenomenon quantitatively, we assigned the ~1700 earthquakes in the 1987–92 period to event clusters using an equivalency class (EC) algorithm (*8*, *9*), and the assignments were further refined by visual inspection and regrouping. The similarity measure, β, used in the EC organization is based on a network-wide characterization of maximum cross-correlation coefficient values for *P* and *S* waves between pairs of earthquakes, and it varies systematically with the distance (offset) separating event pairs (Fig. 2). An unexpected result of this analysis was that the correlated earthquake pairs tended to fall into two distinct, offset-dependent populations. One group (β > 0.9) contains event pairs separated by less than about 200 m, and the other group contains those pairs (β < 0.6) having offsets greater than 500 m. The β versus offset relation seen for the latter group would be expected for a uniform spatial distribution of hypocenters in which waveform similarity slowly decreases with event pair offset because of increasingly different wave propagation paths. The distinct, high β, short-offset group contains the highly similar clustered events. The isolation and intensity of this concentrated group was surprising to us, so we studied it in detail.

We selected a similarity measure of $\beta \geq 0.98$ as our criterion for defining clusters, a value at which the defined cluster population changed little with β. This definition selected 63% of the ~1700 events. These events were found to be organized spatially into 294 small, distinct clusters of 2 to 16 hypocenters that collectively occupy no more than 1% of the active fault surface (Fig. 3). Nearly half (43%) of the clusters contained two events (doublets). For clusters of three or more events, 80 to 90% were complex in that their member events could be further subdivided into subgroups (each containing a different event type) on the basis of subtle differences in high-frequency waveforms. Clustering was more prevalent and tended to be more complex for the shallow earthquakes (*10*).

To investigate the spatial distribution of events within the clusters, we located a representative sample (87 events in 15 clusters) accurately relative to each other by exploiting the similarity of their waveforms (*5*, *11*). This showed that the individual clusters have much smaller dimensions than the 200-m maximum offset for the $\beta > 0.9$ population in Fig. 2 (which is based on our routine absolute hypocenter locations). Half of the clustered events in the sample were found to lie less than 10 m from their respective cluster centroids, and all of the events were within 20 m (*12*). Two shallow clusters, CL14 and CL16 (Fig. 3), containing 14 and 16 members, respectively, demonstrate the types of cluster geometries often seen (Fig. 4). These are complex clusters, each containing three types of events. In CL14, each type has a characteristic size (Fig. 1), spanning about 1.6 in Richter magnitude, whereas the three event types in CL16 are roughly the same size. In both cases each event type appears to occupy a distinct region within the cluster. The clusters define discrete flattened zones, 2 to 5 m thick, of concentrated seismic slip within the fault zone. CL14 is about 35 m long and 7 m wide, with the large events occurring in the upper 20 m of the cluster. CL16 is similar in size, and its event types are organized into groups separated by as little as 2 or 3 m. If we use conventional estimates of rupture dimensions for these earthquakes (*6*), each of the large events of CL14 involved slip over the entire cluster, even though the centroid of energy release appears to be located at a slightly different position for each event.

Another feature of interest regarding events within the clusters was their periodicity in recurrence. We computed the time intervals between successive events

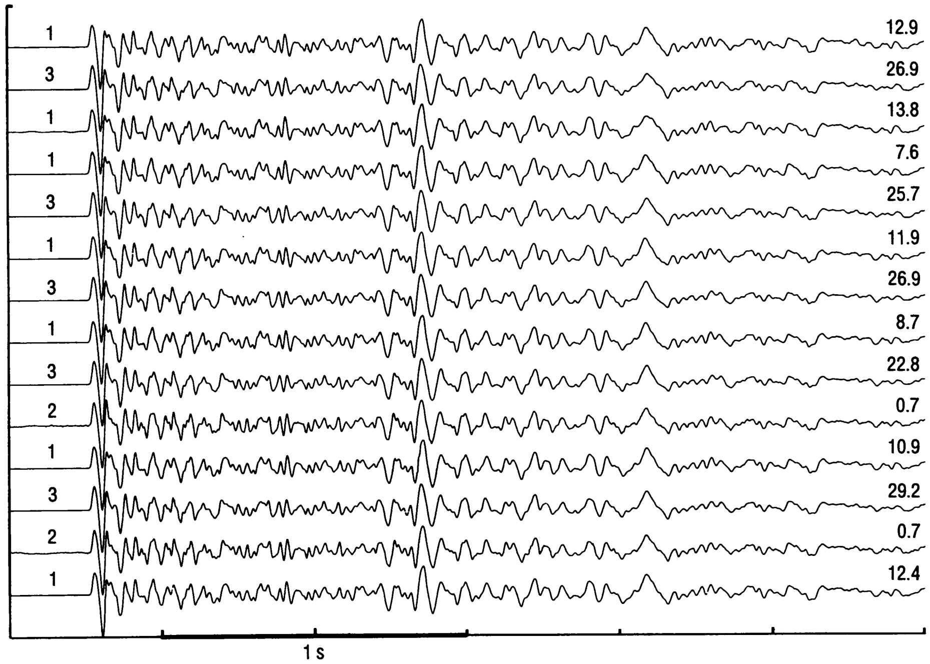

Fig. 1. Vertical-component waveforms recorded at station VCA (see Fig. 3) from cluster CL14, displayed chronologically, most recent on top. Recorded amplitude (counts ÷ 1000) are shown on the right. The cluster subdivides into three types of events on the basis of subtle differences in waveform, as indicated by the numbers on the left.

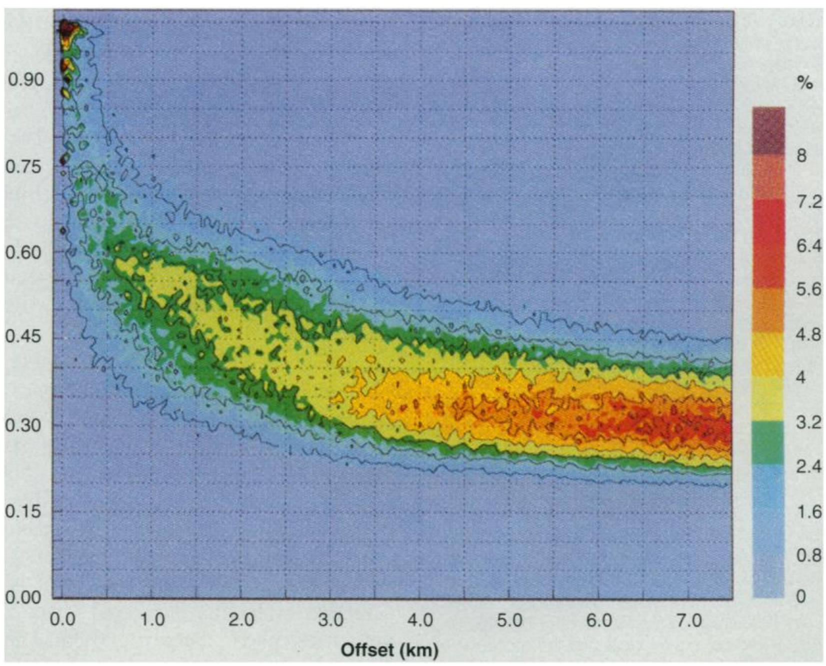

Fig. 2. Cross-correlation measure of similarity, β, versus separation distance (offset) for more than 650,000 event comparison pairs. Permutations of event pairs from 1679 events occurring during the period 1987 to 1992 and separated by 7.5 km or less were used. Earthquakes were located within 5 km of the San Andreas Fault Zone along a 25-km segment centered on the nucleation region of the 1966 *M* 6 mainshock. Contours show the percentage of event comparison pairs with a given offset having a given β. The gap in the range $0.6 < \beta < 0.9$, 200 m < offset < 500 m generally separates highly similar clustered from nonclustered behavior.

(recurrence intervals) in each of the 294 clusters defined by $\beta \geq 0.98$ and found 778 intervals that were bimodally distributed (Fig. 5A). Eighteen percent of the recurrence intervals are less than 0.1 year, and most of these are less than 10 min. These intervals are approximately exponentially distributed (Fig. 5A, inset), much like a typical aftershock sequence. Recurrence intervals between 0.2 and 2.8 years fit a lognormal distribution, as shown in Fig. 5B, with a peak of about 0.8 year. To compare periodic recurrence within these sequences of small earthquakes with recurrence of moderate and large earthquakes (*13*, *14*), we computed the median-normalized recurrence interval, $T/\overline{T}$, for each cluster with two or more intervals longer than 0.2 year. The normalized intervals for all such clusters fit a lognormal distribution closely (Fig. 5C), as do the normalized recurrence intervals for large and moderate earthquakes (*13*). The standard deviation of ln $(T/\overline{T})$ is referred to as the intrinsic uncertainty in the recurrence interval (*14*) and is a measure of the regularity of occurrence (*15*). From Fig. 5C we obtained an intrinsic uncertainty of 0.43, compared with the value of 0.21 used in earthquake forecasting (*14*). However, as we discuss next, recurrence in a complex cluster is often dominated by one type of event, and when only the dominant events in our representative sample of clusters are considered, the intrinsic uncertainty is much smaller, in the range of 0.03 to 0.3, indicating strongly periodic behavior.

Both short-interval (minutes) and long-interval (months) recurrence traits can be seen in simple plots of cluster event occurrence times (Fig. 6). Bursts of near-simultaneous events within complex clusters like CL14 and CL16 invariably involved events of different types; we have yet to observe the near-simultaneous occurrence of events of the same type in a cluster. Events that repeated at intervals of several months, in contrast, were predominantly of one type, although one or more of the other event types in the cluster were often incorporated into the regular sequence as bursts of coincident activity both before and after the dominant repeating event. In CL14 the large-magnitude events dominated the regularity, whereas in CL16 the periodic recurrence pattern (235 ± 25 days, mean ± SD) was produced by the events that fill the central portion of the cell (type 1 in Fig. 4). Repeat times between the dominant CL14 events became progressively shorter. Clusters of a single event type usually exhibited higher periodicity than was generally seen for complex clusters, as shown for CL5 (459 ± 16 days) (Fig. 6), suggesting that interaction among event types in complex clusters interferes with regularity.

The bimodal distribution of recurrence intervals in Fig. 5 is for $\beta \geq 0.98$, which corresponds to event-pair offsets of less than 30 to 40 m. To investigate the distributions at larger offsets, we redefined the clusters for gradually decreasing values of β, progressively merging nearby but presumably out-of-phase periodic clusters and causing the gradual disappearance of the lognormal recurrence peak. Near β = 0.93, a value corresponding to offsets of 100 to 200 m, the number of intervals shorter than 10 min reached a maximum and the bimodal character of the distribu-

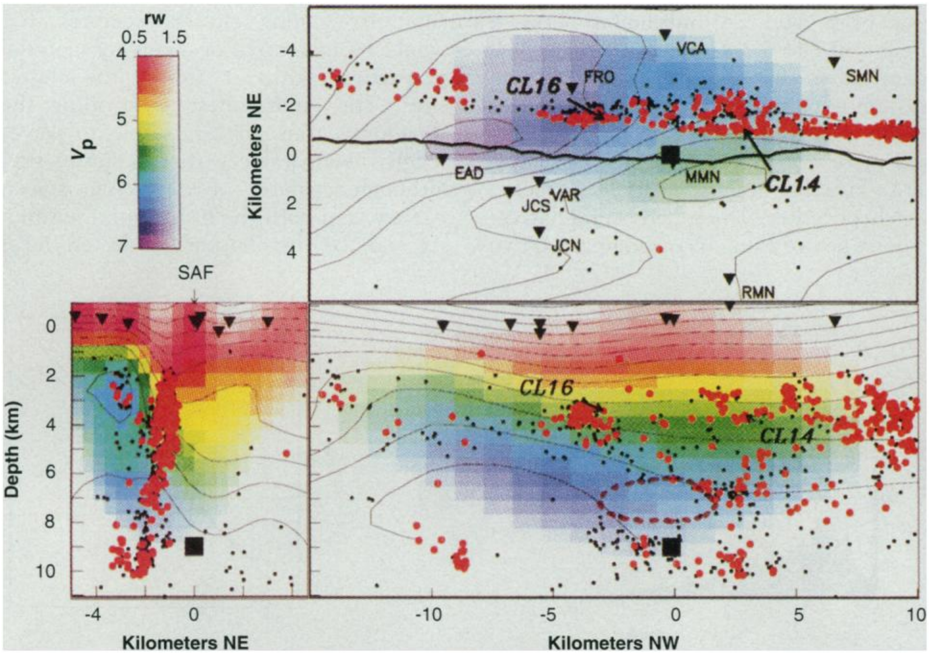

Fig. 3. Sections through the three-dimensional velocity model for Parkfield (*4*) showing the 294 cluster locations (large dots) defined for $\beta \geq 0.98$, background seismicity (small dots), the 1966 main shock (large square), and recording station names and locations (small triangles) projected onto the fault plane. Depth is kilometers below sea level. The V_p contours and the high V_p/V_s anomaly location (dashed contour) are shown.

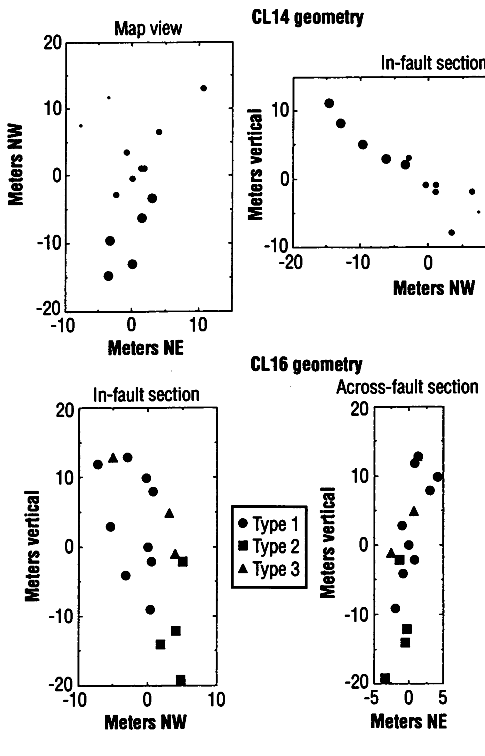

Fig. 4. Cell geometries for example clusters CL14 and CL16. The coordinate system is oriented on the southeast-northwest fault zone with its origin at the centroid of the cluster. Sections are vertical-plane projections onto and normal to the San Andreas fault. In CL14, the event type is indicated by symbol size, which also represents source strength (larger symbols for greater seismic moment). Events in CL16 are all of approximately the same magnitude.

tion vanished. This indicates that there is communication between earthquakes 100 to 200 m apart on a time scale of several minutes, corresponding to communication at speeds of 10 to 100 cm/s.

Having found clustering and patterns in recurrence intervals for small earthquakes, we next examined these features in relation to the depth of the seismic activity. Deeper than about 5 km, clusters were less common, contained fewer events on average, and did not exhibit recurrence intervals of less than 10 min, as was generally seen in many shallow clusters. There was more variation among waveforms for deep clusters than for shallow clusters, possibly because of longer, slightly different propagation paths or physical heterogeneity in the cluster volume, although the separations between deep cluster members are similar to those in shallow clusters. Some communication between deep clusters was evident as sympathetic activity in neighboring clusters at ranges of up to 200 m, but at intervals of hours to days rather than minutes.

To investigate the temporal stability of the clustering process, we examined characteristics of individual clusters as well as the entire seismicity picture throughout the study period. Significant change was found in some aspects of cluster behavior, along with evidence for high stability in other aspects.

Locations of dominant repeating events appeared to migrate cyclically within the clusters over several years (Fig. 6). In CL14, the largest events define one cycle in 6 years, and the dominant events in CL16 define two cycles in the central region of the cluster (Fig. 4). If we can assume that these systematic patterns in space and time are genuine, we are viewing the process of fault slip at a scale approaching 2 to 3 m. The relative hypocenter location technique presumes that the *P* and *S* wave velocities are not changed by earlier nearby earthquakes or other local processes, and that effects such as meter-scale heterogeneity in source mechanisms or medium properties are negligible (*16*). An apparent 20-m migration of a hypocenter could be caused by stress-induced travel-time variations of a few milliseconds that would impress the same migration pattern on all event types within the cluster (*17*). There is some evidence for this in CL16, but it is less pronounced in CL14 (Fig. 6). This phenomenon, if present, would not affect the cluster periodicity or the definition of event types.

We also examined the change with time in the fraction of seismicity represented by clustered earthquakes (Fig. 7). The total number of earthquakes per year increased from 1987 to 1993, but the fraction of all events that were cluster members decreased somewhat, from around 70% of the total to about 60%. The ratio of the number of events deeper than 5 km to the total number of events doubled. The relative sizes of the two peaks in the distribution of recurrence intervals (Fig. 5A) also changed with time. The population in the short-interval peak was growing with time relative to that in the 0.8-year peak, and the minimum between them at 0.1 to 0.2 year became more pronounced, so that the increased seismicity was being partitioned into more near-coincident events within existing clusters and more nonclustered deep events. Recent clustering activity near the expected M 6 hypocenter, which had been relatively quiet before 1992, has accompanied two earthquake sequences at depths of 8 to 10 km with mainshock magnitudes of 4.7 and 4.8.

During the entire observation period, which represents about 25% of the average M 6 recurrence interval at Parkfield, the local stress state presumably was changing as the fault zone was being loaded by the regional tectonic strain. Despite this, we found no progressive changes in waveform similarity among cluster members that would be indicative of changing material properties within or around the cluster sites. The environment controlling the waveforms thus appears stable to wavelengths comparable with the cluster size, although regularity of occurrence is seen to vary, and both the background seismicity and the distribution of clusters have

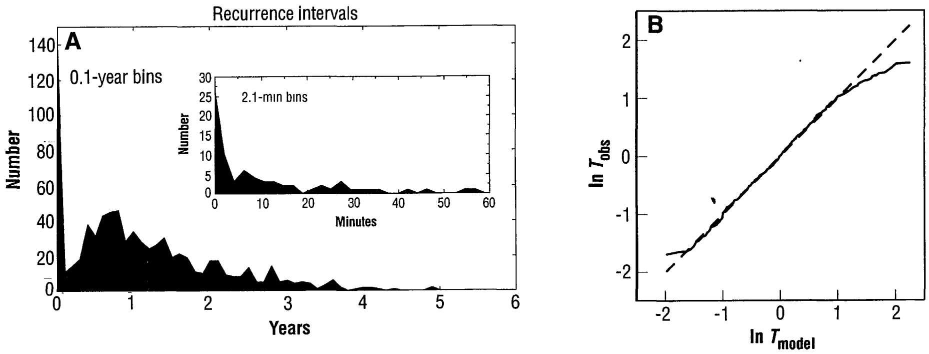

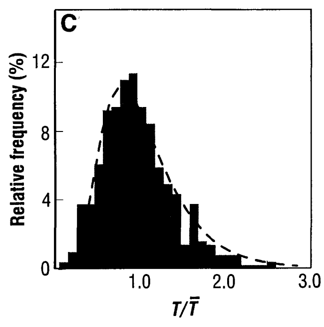

Fig. 5. (**A**) Distribution of intracluster recurrence intervals. The bimodal character of the distribution is shown in the main figure, in which data are plotted in 0.1-year bins. The inset (2.1-min bins) shows details of the distribution of short recurrence intervals, illustrating the peak at intervals less than a few minutes and the approximately exponential fall-off. (**B**) Fit of the distribution of recurrence intervals greater than 0.2 year (solid) to a lognormal model (dashed). Intervals greater than 2.8 years are undersampled because the database is complete only for about 5.5 years, and all intervals are undersampled to some extent because of equipment malfunctions or imperfect event detection. (**C**) Distribution of median-normalized recurrence intervals for clusters with two or more recurrence intervals of 0.2 year or greater and lognormal fit (dashed).

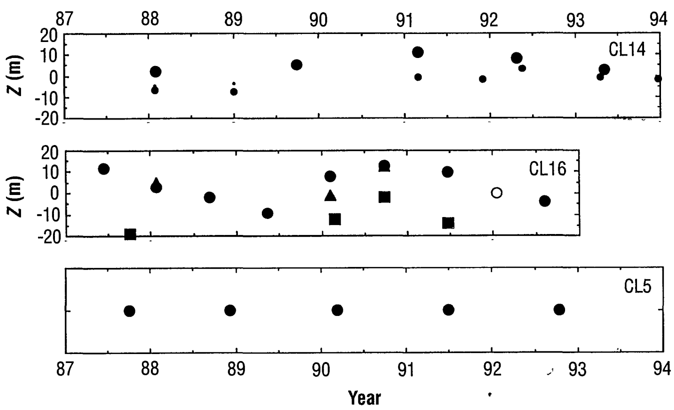

Fig. 6. Event chronology patterns for three clusters (see Fig. 4 for explanations of symbols). Ordinates for CL14 and CL16 are vertical positions of the events with respect to the cluster centroid. Precise hypocenter locations are not available for CL5, so spatial positions are not given. The open circle in the CL16 plot is a type 1 event that could not be located. Note the periodicities in the largest events of CL14 and in the type 1 events of CL16. CL5 illustrates the strong periodicity seen in noncomplex clusters having events of only one type.

changed over the larger scale fault zone.

In an earlier study of a cluster of small similar earthquakes (M ~ 1.5) in central California, the logarithm of the elapsed time since a previous event was found to be proportional to the seismic moment and inversely proportional to the stress drop of the subsequent event (*18*). These observations were explained by progressive healing of the fault between events. We examined a group of 11 clusters for evidence of this phenomenon at Parkfield and found no dependence of elapsed time on moment. Rather, within clusters we found a pattern of periodic recurrence of similar-size events, modified to varying degrees by interactions with other event types in the same cluster.

We have considered some intuitively simple processes that might explain the following observed fault zone phenomena: localized seismicity in small clusters, both quasi-periodic and aperiodic recurrence within clusters, sympathetic occurrence of events up to a range of ~200 m, and clustering behavior that is not stationary.

The clusters localize 63% of the microearthquake activity onto about 300 small patches, with a total area of <1 km^2 and distributed over the 10 km by 25 km fault segment. These sites represent concentrations in strength or in stress that are related to heterogeneity in the mechanical, thermal, chemical, or hydrological properties of the fault zone. Mechanisms of the microearthquakes are predominantly strike-slip motion with San Andreas geometry, regardless of the cluster shape or orientation, indicating that the homogeneous regional stress field controls the slip direction within the clusters. The tendency among the clusters to similar recurrence intervals suggests a common driving mechanism for the periodicity. The simplest mechanism conceptually is frictional stick-slip on cluster patches of constant strength under steady tectonic loading. Alternatively, repeated failure under approximately constant load could occur if the patch strength is modulated locally in a steady-state mode. Near-simultaneous events of differing types within the same cluster are similar to earthquake aftershock sequences but without a defining large-magnitude mainshock. Triggering of events in nearby clusters within a range of 200 m may involve rapid aseismic slip on the fault surface between the clusters. Alternatively, the stress field perturbation from an event in one cluster may be sufficiently intense within a distance of 200 m to induce slip in another cluster. It is difficult to discriminate between these possibilities.

A possible role for fault zone fluids in the earthquake process has been proposed in general (*19*), and at Parkfield specifically (*20*). Common themes involve high pore pressures, rapidly sealing compartments, hydrofracturing, episodic flow, and permeability barriers. Verification of these hypotheses will likely require direct sampling by drilling into one or more of the shallow clusters at a depth of 3 or 4 km (*21*).

Nucleation of the next M 6 earthquake at Parkfield is a steadily evolving process of fault zone deformation that involves periodic recurrence of characteristic microearthquakes that are localized in small clusters. The overall rate of seismicity is increasing, and the fraction of the total seismicity confined to clusters is decreasing. Deeper seismicity is seen to increase markedly with time, whereas activity above 5 km depth appears to be relatively stable. If these trends can be projected, seismicity in the early loading phase is dominated by shallow clustered activity. By the end of the cycle, the increasing seismicity is largely filling zones that were relatively quiet, including the deep site of the impending rupture onset. A rapid decrease in clustering that accompanies increased deep seismicity, therefore, may be an indication of an impending M 6 earthquake.

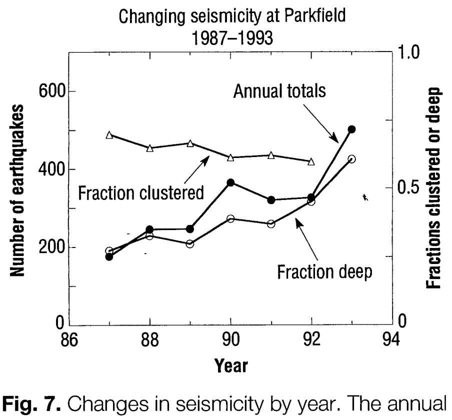

Fig. 7. Changes in seismicity by year. The annual earthquake count increased substantially over the period 1987 to 1993, whereas the fraction of the total number of earthquakes that are clustered events decreased during the analysis period (1987–92). The fraction of the total activity deeper than 5 km increased significantly. The mode of slip in the fault zone is changing, involving more earthquakes in the deep nucleation zone.

REFERENCES AND NOTES

1. Y. Y. Kagan, *Bull. Seismol. Soc. Am.* **83**, 7 (1993); J. McCloskey and C. J. Bean, *Science* **266**, 410 (1994).
2. W. H. Bakun and T. V. McEvilly, *J. Geophys. Res.* **89**, 3051 (1984).
3. W. H. Bakun and A. G. Lindh, *Earthquake Predict. Res.* **3**, 285 (1985).
4. A. Michelini and T. V. McEvilly, *Bull. Seismol. Soc. Am.* **81**, 524 (1991).
5. R. Nadeau, M. Antolik, P. Johnson, W. Foxall, T. V. McEvilly, *ibid.* **84**, 247 (1994).
6. Source parameters conventionally estimated from the source spectrum of a typical small event are as follows: magnitude ~0.5, seismic moment ~0.5 × 10^{17} dyne cm, source radius 5 to 10 m (10 to 20 m for M ~ 1.5), and stress drop 3 to 10 MPa.
7. The frequency spectrum of the P or S wave displacement is flat at low frequency and decreases exponentially beyond the "corner" frequency because of interference due to the finite source. A similar spectral roll-off will be introduced by the source rise time, which is the duration of the slip at a point. Anelastic attenuation due to medium properties also produces high-frequency spectral decay that can mask high corner frequencies, although spectral ratios for co-located events should eliminate this effect.
8. R. C. Aster and J. Scott, *Bull. Seismol. Soc. Am.* **83**, 1307 (1993).
9. D. E. Knuth, *Fundamental Algorithms, The Art of Computer Programming* (Addison-Wesley, Reading, MA, 1968), vol. 1.
10. About 75% of the events above 5 km depth are members of clusters, representing 44% of the total centers of activity (cluster sites plus nonclustered events), compared with only about 40 and 20%, respectively, for the deeper events.
11. M.-J. Frémont and S. D. Malone, *J. Geophys. Res.* **92**, 10223 (1987).
12. These distances approach the spatial resolution of the analysis, so that at least some of the events in clusters may be co-located. Unlike a conventional hypocenter determined from arrival times, which is the point of rupture nucleation, each of these relative locations corresponds to a centroid of seismic moment release, because the cross spectra of entire P or S waveform pulses are used to estimate the time delays between the event arrivals.
13. S. P. Nishenko and R. Buland, *Bull. Seismol. Soc. Am.* **77**, 1382 (1987).
14. Working Group on California Earthquake Probabilities, *U.S. Geol. Surv. Circ. 1053* (1990).
15. An intrinsic uncertainty value of 0 means perfect time predictability. A value of 1 means that the normalized recurrence intervals describe a Poissonian process where recurrence times are not predictable (*14*).
16. Two observations support these assumptions. First, pairs of events from different event types occurred only a few minutes apart in either order, with no measurable effect of the first event on the waveform character of the second. Second, events of different event types in a cluster sometimes were separated by distances much smaller than separations between events of the same type [for example, CL16 (Fig. 4)].
17. Progressive travel-time variations of this magnitude have been reported at Parkfield [E. Karageorgi, R. Clymer, T. V. McEvilly, *Bull. Seismol. Soc. Am.* **82**, 1388 (1992)].
18. J. E. Vidale, W. L. Ellsworth, A. Cole, C. Marone, *Nature* **368**, 624 (1994).
19. M. L. Blanpied, D. A. Lockner, J. D. Byerlee, *ibid.* **358**, 574 (1992); J. Byerlee, *Geology* **21**, 303 (1993); P. Gavrilenko and Y. Gueguen, *Tectonophysics* **217**, 91 (1993); A. H. Lachenbruch, *J. Geophys. Res.* **85**, 6097 (1980); P. R. Sammonds, P. G. Meredith, I. G. Main, *Nature* **359**, 228 (1992); R. H. Sibson, *Tectonophysics* **211**, 283 (1990); A. Nur and J. Walder, in *Fault Mechanics and Transport Properties of Rocks*, B. Evans and T.-F. Wong, Eds. (Academic Press, San Diego, CA, 1992), chap. 19; J. R. Rice, *ibid.*, chap. 20; N. H. Sleep and M. L. Blanpied, *Nature* **359**, 687 (1992); *U.S. Geol. Surv. Open-File Rep. 94-228* (1994).
20. P. A. Johnson and T. V. McEvilly, *J. Geophys. Res.*, in press.
21. S. Hickman, M. Zoback, L. Younker, W. Ellsworth, *Eos* **75**, 137 (1994).

22. The Parkfield High-Resolution Seismic Network functions through close cooperation among researchers at the University of California at Berkeley, Lawrence Berkeley Laboratory (LBL), Duke University, and the U.S. Geological Survey (USGS). USGS provides financial support for this research through National Earthquake Hazards Reduction Program award 14-08-0001-G1703. Data processing was done at the Center for Computational Seismology at LBL, which is operated by the University of California for the U.S. Department of Energy under contract No. DE-AC03-76SF00098.

2 September 1994; accepted 28 November 1994